Reactivity of Coinage Metal Hydrides for the Production of H_2 Molecules

Iñigo Iribarren,[a] Goar Sánchez-Sanz,[b] José Elguero,[c] Ibon Alkorta,*[c] and Cristina Trujillo*[a]

The formation of molecular hydrogen as well as the possibility of using coinage metal hydrides as a prospective complex to produce hydrogen was presented in this work. Therefore, the reactions involving the interaction between two coinage metal hydrides, MH (M=Cu, Ag and Au, homo and heterodimers), were studied. The free energy profiles corresponding to aforementioned complexation were analysed by means of ab initio methods of quantum chemistry. The characteristics of these intermediates, final complexes and the electron density properties of the established interactions were discussed.

1. Introduction

Hydrogen storage is a key enabling technology for the development of hydrogen and fuel cell-based economy. Hydrogen is an attractive energy carrier because it is carbon-free and therefore without CO_2 emissions and has an exceptional mass energy density.[1]

Unfortunately, hydrogen is an extremely volatile gas under ambient conditions, resulting in a volumetric energy density that is much too low for practical applications. For on-board use, hydrogen must be compressed to very high pressures or stored cryogenically, both of which cost energy and substantially increase vehicle weight. As a direct consequence, efficient and cost-effective storage of hydrogen remains a challenge.[1] In this context, chemical hydrogen storage materials have produced a plethora of investigations with particular attention to the design of low-cost materials that can reversibly and rapidly store hydrogen near ambient conditions at a density equal to or greater than liquid hydrogen.[2] Metal hydride materials research has been focused on improving both the volumetric and gravimetric capacities, hydrogen absorption/desorption kinetics, and reaction thermodynamics of potential material candidates.[3]

The use of metals and metallic cluster to trap/storage hydrogen molecules from the theoretical perspective has been widely studied. Some, but not limited to, examples can be found for Mg and MgH_2,[4] $Mn_4O_4^+$,[5] Mn_xO_{x+y},[6] $Ca_nMn_{(4-n)}O_n$,[7] Na_xB_y clusters,[8] etc. The opposite process characterised by the molecular hydrogen dissociation on gold clusters was studied by means of using density functional theory in 2009.[9] In 2016, a computational study of the H_2 activation process at coinage metals (Cu, Ag and Au) of the corresponding fluorides, MF (M=Cu, Ag and Au), and its splitting leading to the M–H···H–F dihydrogen bonded complex was performed by Grabowski and Ruipérez.[10]

In fact, the use of coinage metals, interacting with H_2 in $M(H_2)_n^+$ clusters (M=Cu, Ag and Au) has been also recently studied,[11] highlighting the capacity of coinage-metal hydrides to hydrogenate CO_2.[12]

Herein, the process involving the interaction of coinage metal hydrides, MH (M=Cu, Ag and Au, homo, and heterodimers) to produce and therefore storage H_2 molecule, and its splitting leading to isolated dihydrogen systems is the aim of this study (Scheme 1). The characteristics of the reaction pathways corresponding to the formation of molecular hydrogen, including intermediates and transition states, and the possibility of the products to act as hydrogen storage molecules are analysed by means of ab initio methods of quantum chemistry, from both thermodynamic and kinetic perspectives. In addition, the nature of the interactions established in the complexes and the bond characterisation was analysed.

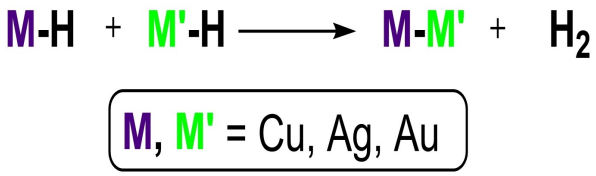

Scheme 1. Reaction under study in gas phase.

[a] I. Iribarren, Dr. C. Trujillo
Trinity Biomedical Sciences Institute
School of Chemistry
The University of Dublin
Trinity College
Dublin 2 (Ireland)
E-mail: trujillc@tcd.ie
[b] Dr. G. Sánchez-Sanz
Irish Centre of High-End Computing
Grand Canal Quay
Dublin 2 (Ireland)
& School of Chemistry
University College Dublin
Belfield, Dublin 4 (Ireland)
[c] Prof. J. Elguero, Prof. I. Alkorta
Instituto de Química Médica IQM-CSIC
Juan de la Cierva, 3
28006 Madrid (Spain)
E-mail: ibon@iqm.csic.es

Supporting information for this article is available on the WWW under https://doi.org/10.1002/open.202100108

2. Results and Discussion

We began by calculating the free energy profile associated to the reaction between coinage metal hydrides as illustrated in Scheme 1. All the six possible reactions were contemplated, which corresponds to three homodimer reactions (M–H + M–H) and three heterodimer reactions (M–H + M′–H).

2.1. Homodimers

First, we will focus on the reactivity between homodimers, *i.e.* two identical M–H molecules. Two different orientations of both interacting monomers were considered and described in Scheme 2. From the entrance channel, the reactants can interact whether in a parallel or in a perpendicular way, leading to two different pre-transition state assembly complexes, **A** and **B** respectively (Scheme 2).

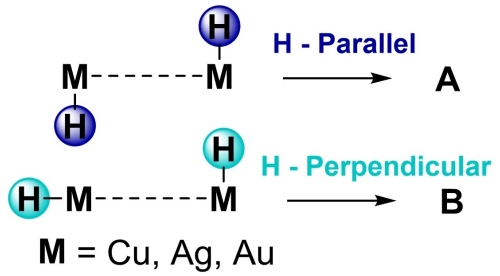

Scheme 2. Two different types of orientations for monomers parallel or perpendicular.

The free energy profiles corresponding to the three different homodimer reactions were studied in gas phase. In Figure 1 the energy profile of $(Ag–H)_2$ has been plotted (Table 1), the potential energy surfaces corresponding to M=Cu and M=Au can be found in Figure S1 in the Supporting Information.

The energy profiles for the reaction between both monohydrides for the three coinage metals indicate that both **A** and **B** intermediates can be obtained directly from the entrance channel. However, interestingly the conversion between **A** and **B** is also possible due to the existence of a transition state between both. In all cases, intermediate **B** is much more stable than intermediate **A**, and in addition, the transition barrier corresponding to the **A**–**B** conversion is very low. Therefore, despite that both intermediates are energetically accessible from the interaction between monomers; **B** will be the preferable intermediate. From **B**, both the hydrogen atom in between both metals will be transferred to one of them, giving rise to complex **C**. Due to the height of the transition **B**–**C** barrier; this is the rate-determining step of the reaction. This energetic barrier (**tsBC**) is 136 and 138 $kJ \cdot mol^{-1}$ both for Cu and Ag, respectively, and 60 $kJ \cdot mol^{-1}$ for the reaction involving Au–H monomers. Although the barriers involving the transfer of one single hydrogen atom, **B** to **C** process, are relatively high, complex **C** is very stable, particularly when M=Ag and Au, being the driving force of the reaction. Finally, the stability of the M–M + H_2 process concerning the release of hydrogen molecule was studied, named **D** in the energy profile. For Cu and Au, the intermediate **C** is more stable than **D**; therefore, the process involving the release of hydrogen molecule is less likely and the **C** intermediate (M=Cu and Au) present good features to retain H_2. However, when the silver metal is implicated, **D** product in where the molecule of H_2 is released, is slightly more stable than **C**, consequently the possibility to release free H_2 becomes more plausible. These results agree with the regium bonds strength trend observed between homodimers and Lewis bases ($Au_2 > Cu_2 > Ag_2$).[13]

In terms of the geometries of the two different intermediates, **A** and **B** (Figure 2), it is worth mentioning that for the gold

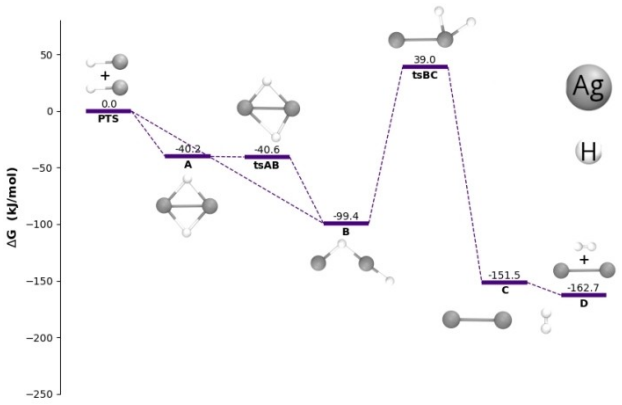

Figure 1. Free energy profile for the reaction involving AgH monomers. **D** corresponds to the Ag_2 and H_2 molecules at the dissociation limit. All the free energies (in $kJ \cdot mol^{-1}$) were obtained at MP2/aug-cc-pVQZ//aug-cc-pVTZ.

Table 1. Free relative energies (ΔG, $kJ \cdot mol^{-1}$) calculated at the MP2/aug-cc-pVQZ//aug-cc-pVTZ computational level.

Complex	ΔG $kJ \cdot mol^{-1}$		
	Cu	**Ag**	**Au**
A	−77.3	−40.2	−76.7
tsAB	−73.7	−40.6	−71.4
B	−120.0	−99.4	−84.9
tsBC	16.5	39.0	−24.0
C	−102.9	−151.5	−130.0
D	−80.5	−162.7	−78.2

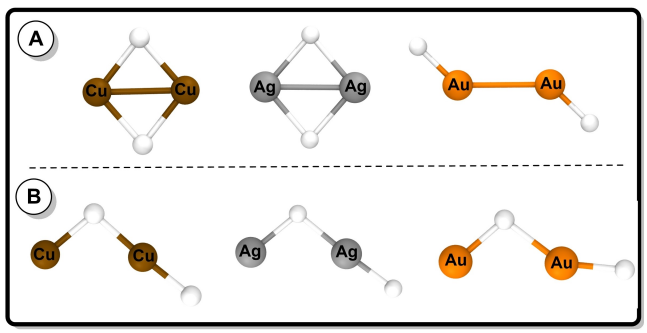

Figure 2. Optimised geometries for **A** and **B** complexes at MP2/aug-cc-pVTZ computational level

homodimers, a different structure for **A** was obtained than those found for copper and silver homodimers.

In Table 2, the M–M and M–H distances for all the minima under study are summarised. Regarding the distance between both coinage metal atoms, intermediate **B** presents the longest M–M distance in all cases. When M–H is revised, for Cu atom, M–H bond is shorter along the pathway reaction, while for Ag and Au, M–H distance decreases from **A** to **B** but increases when **C** is obtained. In fact, in the case of Ag derivatives, M–H distance in C is 2.10 Å, the longest Ag–H for the whole $(Ag–H)_2$ pathway. This finding agrees with the fact that the H_2 production process is only favourable for Ag coinage metal. It is noteworthy to mention that the step involving **B** to **C** transformation is not reversible for Ag and Au, while for Cu, **C** is slightly less stable than **B** complex.

2.1.1. Bonding Characterisation

It is clear that going from the intermediate **A** to **B** along the reactive pathway, the M–M distance increases for all cases, and once the intermediate **C** is achieved the M–M distance decreases again. That can indicate a destabilisation of the M–M bond from **A** to **B** with a subsequent stabilisation of the M–M bond in **C**. Therefore, in order to describe the interaction between coinage metals within the different intermediates, the QTAIM was used to characterise those M–M bonds. Several studies have shown that QTAIM descriptors such as electron density values at bond critical points (BCPs) may often be treated as measures of the strength of the hydrogen bond.[14] The distances and all the values for the density and the Laplacian corresponding to the M–M bonds were summarised in Table 3 (values of the electron density description at the BCP for the rest of interactions can be found in Table S2, ESI).

Table 2. Distances M–M and M–H for the minima (Å) calculated at the MP2/aug-cc-pVTZ computational level.

Bond		A			B	
Å	Cu	Ag	Au	Cu	Ag	Au
M–M	2.13	2.46	2.51	2.32	2.65	2.60
M–H1	1.68	1.90	1.51	1.52	1.69	1.58
M–H2	1.67	1.90	1.51	1.47	1.62	1.56
Bond		**C**			**D**	
Å	**Cu**	**Ag**	**Au**	**Cu**	**Ag**	**Au**
M–M	2.21	2.49	2.42	2.20	2.49	2.43
M–H1	1.61	2.10	1.68	-	-	-
M–H2	1.61	2.10	1.68	-	-	-

Table 3. Electron density at the M–M BCP (ρ), Laplacian ($\nabla^2\rho$), and intramolecular distance (Å) for all the complexes studied at the MP2/aug-cc-pVTZ computational level.

	Complex	ρ	$\nabla^2\rho$	D[M–M]
Cu	**A**	0.0839	0.2433	2.131
	B	-	-	2.318
	C	0.08129	0.1168	2.194
Ag	**A**	0.0683	0.23078	2.459
	B	-	-	2.651
	C	0.06993	0.17848	2.467
Au	**A**	0.0820	0.2093	2.512
	B	-	-	2.598
	C	0.1048	0.1852	2.425

As observed, three different types of bonds were identified, H–H, M–H and M–M, respectively, noting that the M–M bonds presents the lowest density value (Figure 3). For the intermediate **B**, no BCP between both metals was located, being the M–M distance longer than for **A** and **C** cases, *e.g.* in Ag derivatives, intermediate **B** is almost 0.2 Å longer compared with **A**. As it is shown in Figure 3, an excellent exponential relationship was found for the M–H bond for the three families of compounds.[15]

Summarising, BCPs were found between both metals within intermediates **A** and **C** but not for intermediate **B**, which suggest that no bond was established between the two metals for the latter. However, the absence of a BCP does not imply the absence of any interaction. To provide with another verification of the existence/absence of M–M metal interactions within intermediates **B**, an analysis of the M–M bond within **B** by means of the Independent Gradient Model (IGM) developed by E. Henon et al. was performed.[16] The existence of an interaction between both metal atoms will be illustrated by a 3D isosurface in between both corresponding atoms. Same wise, the absence of such area will indicate that no interaction occurs. For the sake of clarity, only graphs for **M=Ag** are depicted in Figure 4, but we obtained similar results for the different homodimer complexes under study (see Figure S3 in the Supporting Information).

Using the isosurface value of $\delta g = 0.1$ a.u. was selected for the study, it is observed that intermediate **A** exhibits a green

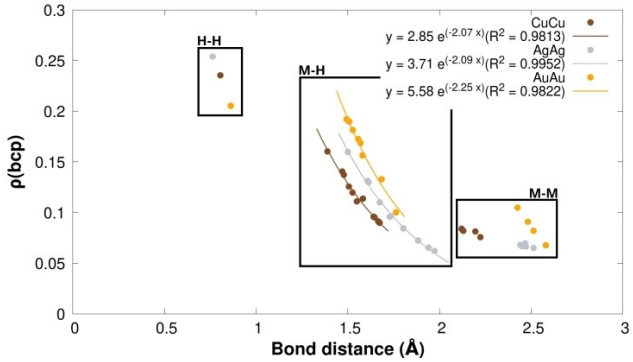

Figure 3. Exponential correlation density at BCPs *vs.* bond distances (H–H, M–H and M–M, going from left to right) regarding the three different homodimers under study for the minima and TSs involved in the energy profile

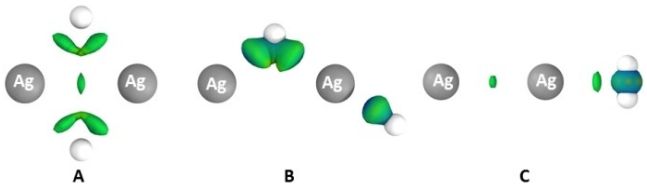

Figure 4. IGM analysis of the $(AgH)_2$ minima $\delta g = 0.1$ a.u. 3D isosurfaces; colour coding in the range $-0.3 < \text{sign}(\lambda_2)\,\rho < 0.3$ a.u. (red and blue, respectively); MP2/aug-cc-pVTZ level of theory

area in between both Ag atoms which evidencing the existing bond. Furthermore, the Ag–H bond is also observed in the green region between Ag and H atoms. Similar features were found for intermediate **C**, again corroborating what it was previously found. However, in the case of the intermediate **B** no intramolecular green isosurface between coinage metals was observed which indicates the absence of such interaction or bond.

2.2. Heterodimers

Once the homodimers cases were analysed, the heterodimer scenario, M_1–H + M_2–H ($M_1 \neq M_2$) was addressed. As it happened within the homodimers, two different interaction modes were considered, parallel and perpendicular (Scheme 3). Curiously, in the heterodimers' cases, intermediate **A** was not found for any metal under study. However, since two different metals were considered, two different intermediates **B**, $\mathbf{B_{M1}}$ and $\mathbf{B_{M2}}$, were obtained regarding which of the metal the hydrogen atoms are bound to, $\mathbf{M_1}$ or $\mathbf{M_2}$, respectively (Scheme 3).

The three different energy profiles were investigated, with two energetic pathways for each heterodimer reaction: one corresponding to the $\mathbf{B_{M1}}$(indigo) intermediate and the other one to $\mathbf{B_{M2}}$(lime) (Figure 5 and Figures S4–S5 in the Supporting Information, respectively. Values gathered in Table 4). From the entrance channel both $\mathbf{B_{M1}}$ and $\mathbf{B_{M2}}$ were obtained. It is worth noting that, unexpectedly, a transition state between the two **B** intermediates, $\mathbf{tsB_{M1}}$-$\mathbf{B_{M2}}$, was found for the reactions involving, **AgH**–**CuH** and **AuH**–**AgH** heterodimers. Intermediates **B** (Figure 6) will lead to two different **C** intermediates, in which both hydrogen atoms are bound to one of the metals, $\mathbf{C_{M1}}$(indigo) and $\mathbf{C_{M2}}$(lime), respectively.

From the potential surface involving **Au**–**H** interacting with **Ag**–**H** (Figure 5) or **Cu**–**H** (Figure S5 in the Supporting Information), it is clear that the first step heads towards to the intermediate $\mathbf{B_{Au}}$ (the calculated Boltzmann population for $\mathbf{B_{Au}}$ is 99% in both cases). Thus, despite $\mathbf{C_{Au}}$ is thermodynamically less stable than $\mathbf{C_{Ag}}$ (or $\mathbf{C_{Cu}}$), the pathway leading to $\mathbf{C_{Au}}$ is the most favourable one (Figure 5). It is worth mentioning that for the **Au**–**H**–**Cu**–**H** case, no transition state between the two different **B** complexes, $\mathbf{B_{Au}}$ and $\mathbf{B_{Cu}}$, was found. Furthermore, for this particular reaction, since $\mathbf{C_{Au}}$ is less stable than $\mathbf{B_{Au}}$ the interconversion would be reversible (Figure S5 in the Supporting Information). For the reaction involving Cu–H and Ag–H heterodimers (Figure S4 in the Supporting Information), Cu atom seems to have more affinity for the hydrogen atoms, being $\mathbf{B_{Cu}}$ and $\mathbf{C_{Cu}}$ the most stable intermediates. Therefore, amongst the three different heterodimers formed, intermediates with Ag atoms seem to be less stable when the hydrogen is bound to Ag. Also, It is noteworthy that for the heterodimer pathways: **AuH**–**CuH** and **AuH**–**AgH**, the final product, **D**, is more stable than $\mathbf{C_{Au}}$ (preferred pathway), therefore the process

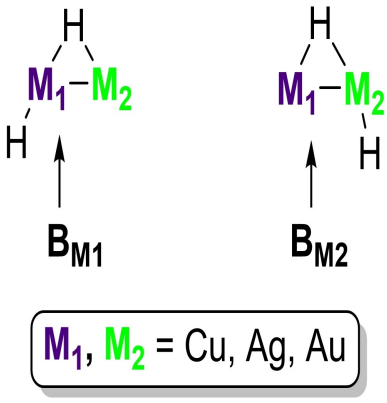

Scheme 3. Two possible intermediates B, B_{M1} and B_{M2}, in the heterodimers reaction.

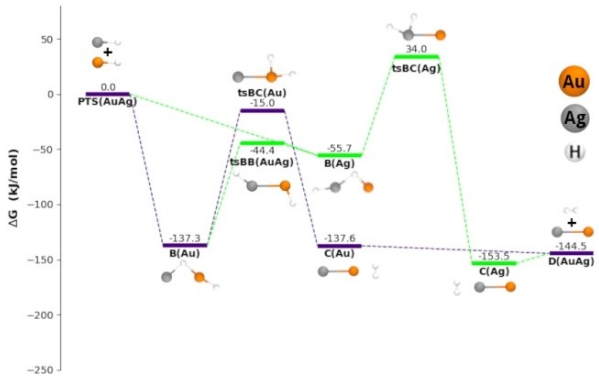

Figure 5. Free energy profile for the reaction involving **AgH** and **AuH** monomers. **D** corresponds to the AuAg and H_2 molecules at the dissociation limit. All the free energies (in kJ·mol^{-1}) were obtained at MP2/aug-cc-pVQZ//aug-cc-pVTZ

Table 4. Free relative energies (ΔG, kJ·mol^{-1}) calculated at the MP2/ aug-cc-pVQZ//aug-cc-pVTZ computational level.

Complex	ΔG kJ·mol^{-1}		
	$\mathbf{M_1}$=Ag $\mathbf{M_2}$=Cu	$\mathbf{M_1}$=Au $\mathbf{M_2}$=Cu	$\mathbf{M_1}$=Au $\mathbf{M_2}$=Ag
$\mathbf{B_{M1}}$	−95.1	−134.5	−137.3
$\mathbf{B_{M2}}$	−120.4	−73.3	−55.7
$\mathbf{tsB_{M1}}$-$\mathbf{B_{M2}}$	−43.2	N/A	−44.4
$\mathbf{tsB_{M1}}$-$\mathbf{C_{M1}}$	78.4	15.9	−15.0
$\mathbf{tsB_{M2}}$-$\mathbf{C_{M2}}$	−20.0	−41.1	34.0
$\mathbf{C_{M1}}$	−110.3	−111.3	−137.6
$\mathbf{C_{M2}}$	−143.5	−175.6	−153.5
D	−123.1	−118.6	−144.5

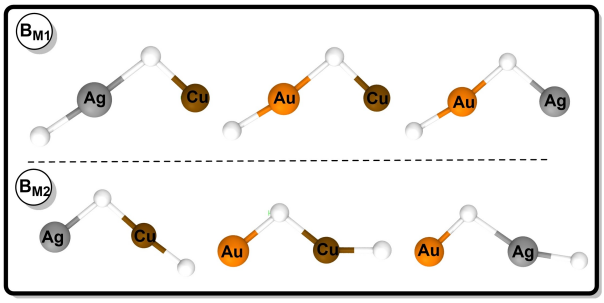

Figure 6. Optimised geometries for $\mathbf{B_{M1}}$ and $\mathbf{B_{M2}}$ complexes at MP2/aug-cc-pVTZ

to release H_2 is favoured (but in all cases **D** is less stable than $\mathbf{C_{M2}}$) The energetic differences between the **C** and **D** complexes are in agreement with those reported for the regium bonds of these heterodimers and five Lewis bases.[13b]

2.2.1. Kinetic Study

Some of the heterodimers under study presented an unexpected transition state between both intermediates **B**. In order to obtain the whole picture of the reactivity, a kinetic study was carried out for those cases.

From the kinetic study for the heterodimer involving **Cu** and **Ag** metals (Figure 7), it is observed that the amount of $\mathbf{B_{Cu}}$ present decreases to become $\mathbf{C_{Cu}}$, being the latter the only kinetic product. From the energetic perspective we obtained that $\mathbf{C_{Ag}}$ is less stable than $\mathbf{C_{Cu}}$ (ca. 33 kJ·mol^{-1}) and the energetic barrier for the reversible path going from $\mathbf{B_{Ag}}$ to $\mathbf{B_{Cu}}$ (~52 kJ·mol^{-1}) is more favourable than the production of $\mathbf{C_{Ag}}$ (**tsBC$_{Ag}$** barrier ~173 kJ·mol^{-1})

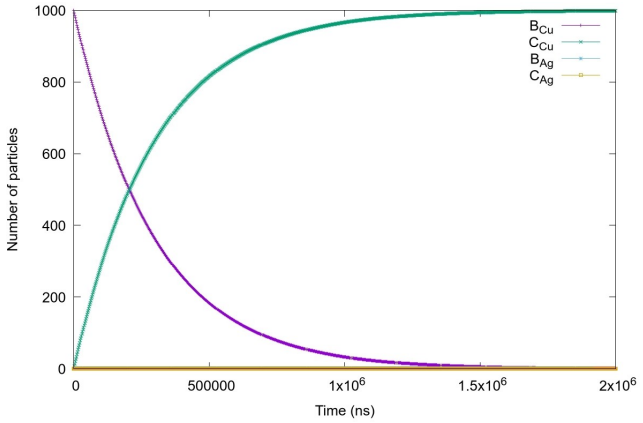

Figure 7. Stochastic simulation for the complex involving the CuH and AgH monomers performed with N = 1000 and $t_{max} = 2\times10^6$ ns. The lines correspond to the number of particles of each species at a certain moment.

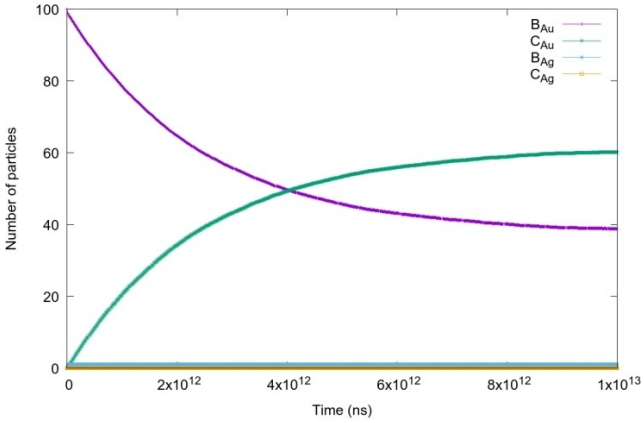

Figure 8. Stochastic simulation for the complex involving the AgH and AuH monomers performed with N = 1000 and $t_{max} = 10^{13}$ ns. The lines correspond to the number of particles of each species at a certain moment

For the **AuH**–**AgH** case (Figure 8), there is a conversion (but not fully) between $\mathbf{B_{Au}}$ and $\mathbf{C_{Au}}$, and both species are coexisting at the end. This result is in an excellent agreement with the energies obtained from the profile study since the calculated Boltzmann population for both complexes is 60%–40% for the corresponding $\mathbf{C_{Au}}$ and $\mathbf{B_{Au}}$.

After the characterisation of the process from the kinetic perspective, even though there are thermodynamic TS located between the two $\mathbf{B_{M1}}$ and $\mathbf{B_{M2}}$ intermediates, no interconversion between them will take place, since the process for the transformation involving $\mathbf{B_M}$ to $\mathbf{C_M}$ is more favourable.

Finally, when the **Au**–**H**–**Cu**–**H** process is studied by means of kinetic principles, the only possible product corresponds to $\mathbf{B_{Au}}$, reinforcing the possibility of the reversibility for the process already discussed (Figure S3 in the Supporting Information).

2.2.2. Bonding Characterisation

For the heterodimer cases the QTAIM analysis was performed to analyse and characterise the nature of the bonds within the intermediates found along the potential energy surfaces and their corresponding molecular graphs have been included in Figure S6 in the Supporting Information. The electron density values and Laplacian at the BCPs and intramolecular distances have been gathered in Table S5 in the Supporting Information. The relationships between ρ_{BCP} and the intramolecular distance for the intermediates of the three possible scenarios were plotted Figure S7 in the Supporting Information. As occurred in the homodimers, similar correlations were found for the heterodimer cases, for H–H, M–H, M'–H and M–M' bonds.

Similarly to what it was found in the homodimers' pathways, intermediate B does not present any bond between both metal atoms. To verify the absence of the M–M bond in **B**, an Independent Gradient Model (IGM) analysis was carried out. The results were summarised in Figure 9 (**AuH**–**AgH**) and Figure S8 (**AuH**–**CuH** and **AgH**–**CuH**). The IGM analysis corroborated that no interactions between M and M' were found in intermediate **B** and only for intermediates **C**, an isosurface between coinage metals was found.

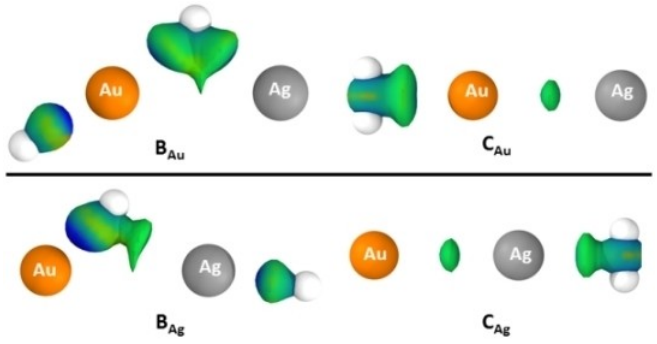

Figure 9. IGM analysis of the (**AgH**–**AuH**) minima $\delta g = 0.1$ a.u. 3D isosurfaces; colour coding in the range $-0.3 < \text{sign}(\lambda 2)\,\rho < 0.3$ a.u. (red and blue, respectively); MP2/aug-cc-pVTZ level of theory

2.3. Molecular Electrostatic Potential

To provide with a further explanation of the behaviour of the coinage metals when interacting one another, the molecular electrostatic potential (MESP) for all the different monomers (**M–H**, **M–M** and **M–M'**) was analysed. All the maxima and minima values on the 0.001 a.u. electron density isosurface were summarised in Table 5 and the MEPS maps plotted in Figure 10 and Figure S9 in the Supporting Information.

In the case of M–H monomers, two maxima were located for each monomer along the M–H axis, one corresponding metal σ-hole ($V_{M,min}$) and another to the H atom ($V_{H,max}$), and one minimum (V_{min}), located close to the H atoms (on Cu–H) or almost perpendicular to the M–M bond in M–M and M–M′ monomers (Figure S9 in the Supporting Information). The σ-hole associated with the Cu atom ($V_{M,max}$) become much deeper (positive) than for Ag–H and Au–H. Besides, the maximum at the hydrogen centre ($V_{H,max}$) presents a positive value in Au–H monomer while for the other two metal hydrides is negative. This fact has been previously reported by Grabowsky and Ruipérez.[10] and it was explained concerning the Pauling electronegativity of the coinage metals. While the electronegativity for the Au atom (2.54) is greater than that of H (2.20), the electronegativity values for Cu and Ag toms, are very similar (1.90 and 1.93, respectively), and smaller than that of hydrogen. In terms of reactivity, those MEPS features, particularly for **AuH** where the σ-hole is the least positive concomitantly with a positive MEP maximum value on the H side, may be the reason behind the different reactivity found for **AuH** with respect to the **AgH** and **CuH**.

It is also noteworthy to mention that for **AuH** monomer, the minimum value (V_{min}) is almost three times smaller (more positive) than those for the **CuH** and **AgH** monomers, and therefore these results have implications within the interaction upon complexation.

For example, in the homodimer case (AuH–AuH), the optimised geometry of intermediate **A** is the result of the interaction between two positive regions, and therefore the hydrogen atoms are in a disposition in where they minimise the electronic repulsion with the Au of the other **AuH** unit. Besides, it can be seen that overall, the energy profile depicted for **AuH–AuH** reaction through **A** is the most favourable one.

When the scenario involving heteroatoms is considered, for the three different energy profiles studied, $\mathbf{B_{Au}}$ is more stable the corresponding to the other metal, being even more dramatic for the **AuH–AgH** with a difference of energy of 122 kJ·mol^{-1} between both complexes **B**.

Table 5. Maxima and minima values of the molecular electrostatic potential (in a.u.) on the 0.001 a.u. electron density isosurface for all the monomers (**M–H** and **M–M'**) calculated at MP2/aug-cc-pVTZ level.

Molecule (AB)	($V_{A,max}$)	($V_{B,max}$)	(V_{min})
CuH	0.1292	−0.0249	−0.0308
AgH	0.1028	−0.0242	−0.0304
AuH	0.0977	0.0220	−0.0132
CuCu	0.0474	0.0474	−0.0232
AgAg	0.0402	0.0402	−0.0207
AuAu	0.0505	0.0505	−0.0180
AgCu	0.0475	0.0404	−0.0218
AuCu	0.0120	0.0927	−0.0274
AuAg	0.0072	0.0788	−0.0270

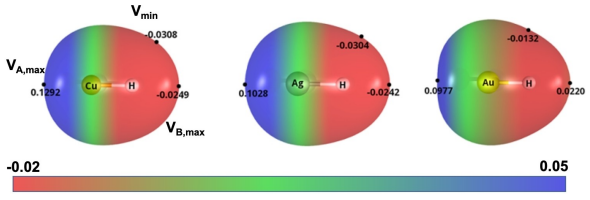

Figure 10. Molecular electrostatic potential on the 0.001 a.u. electron density isosurface for Cu–H, Ag–H and Au–H monomers at the MP2/aug-cc-pVTZ computational level. Maxima and minima critical point are shown in black dots. Colour range: −0.02 (red) to 0.05 (blue) a.u.

3. Conclusions

In summary, the possibility of generating H_2 was investigated by a thorough theoretical study of the reaction performed between two coinage metal hydrides MH (M=Cu, Ag and Au, homo and heterodimers).

Regarding the homodimer scenario, **C** intermediate, in where both hydrogen atoms are connected to one of the coinage metals, was found to be remarkably stable when M=Au and Cu is implicated, being the driving force of the reaction. Therefore, intermediate **C** is likely to retain and possibly store H_2 molecules. However, when the silver metal is implicated, the difference between **C** and **D** complexes is lower and consequently the possibility to obtain free H_2 increases.

Finally, the heterodimer cases were studied. From the potential surface involving **Au–H** the pathway leading to $\mathbf{C_{Au}}$ is the most favourable one. For the reaction involving **Cu–H** and **Ag–H** heterodimers, Cu metal is the chosen to bind to the hydrogen atoms, $\mathbf{B_{Cu}}$ and $\mathbf{C_{Cu}}$. Therefore, amongst the three different heterodimers intermediates formed, Ag metal is the less favourable option as a H_2 reserve. As a general trend, the process in where the coinage metal is acting as a reserve of the hydrogen molecule is, in general, a favoured process, since **B** is more stable than **B**. It is noteworthy that for the heterodimer systems, **AuH–CuH** and **AuH–AgH**, **D** is more stable than $\mathbf{C_{Au}}$, therefore the process leading to H_2 molecule free is favoured.

4. Computational Methods

The structures of the systems under study, minimum and transition states, were optimised at the MP2(full)[17]/aug-cc-pVTZ[18]/aug-cc-pVTZ-PP[19] computational level. Harmonic vibrational frequencies were computed at the same level used for geometry optimisation in order to confirm that the stationary points are either local minima or transition states. Calculations were performed using Gaussian16 software. Single points energies at higher level were computed using the MP2(full)/aug-cc-pVQZ/aug-cc-pVQZPP computational level. Relative free energies (ΔG) were calculated as a difference of the energy of

the optimised complex minus the energy of each monomer in their optimised geometry. The free energies reported in the document were obtained by adding the free energy correction from the small basis set calculations to the potential energy obtained from the high-level single-point energy calculations.

Relative energies (ΔE) were calculated as the difference between the energy of the optimised system and the energy of each monomer in its optimised geometry. The molecular electrostatic potential (MEP) of the isolated monomers was calculated on the electron density isosurface of 0.001 a.u. This isosurface was shown to resemble the van de Waals surface. These calculations were carried out using Gaussian16 software[20] and the numerical results were analysed using the Multiwfn program[21] and plotted using Jmol. The quantum theory of atoms in molecules (QTAIM)[22] was used to analyse the electron density of the systems with the AIMAll program. The Independent Gradient Model (IGM) was used too in order to analyse deeper the electron density of the systems with the IGMPLOT program.[16a–d] The kinetic study of each reaction was used to analyse how the different systems are evolving over time and performed using the Multiscale-KMC software.[23]

Acknowledgements

The research was financially supported by the Spanish Ministerio de Ciencia, Innovación y Universidades (Projects PGC2018-094644-B-C2), Comunidad de Madrid (PS2018/EMT-4329 AIRTEC-CM) and Science Foundation of Ireland (SFI), grant number 18/SIRG/5517. For the purpose of Open Access, the author has applied a CC BY public copyright licence to any Author Accepted Manuscript version arising from this submission. Thanks are given to the CTI (CSIC) and the Irish Centre for High-End Computing (ICHEC) for their continued computational support. We would like to thank Dr. José A. Gámez for all useful ideas and discussions.

Conflict of Interest

The authors declare no conflict of interest.

Keywords: hydrogen storage · coinage hydrides · QTAIM

[1] a) A. Ahmed, S. Seth, J. Purewal, A. G. Wong-Foy, M. Veenstra, A. J. Matzger, D. J. Siegel, *Nat. Commun.* **2019**, *10*, 1568; b) A. Ahmed, Y. Liu, J. Purewal, L. D. Tran, A. G. Wong-Foy, M. Veenstra, A. J. Matzger, D. J. Siegel, *Energy Environ. Sci.* **2017**, *10*, 2459–2471; c) J. Yang, A. Sudik, C. Wolverton, D. J. Siegel, *Chem. Soc. Rev.* **2010**, *39*, 656–675.
[2] L. J. Murray, M. Dincă, J. R. Long, *Chem. Soc. Rev.* **2009**, *38*, 1294–1314.
[3] J. Bellosta von Colbe, J.-R. Ares, J. Barale, M. Baricco, C. Buckley, G. Capurso, N. Gallandat, D. M. Grant, M. N. Guzik, I. Jacob, E. H. Jensen, T. Jensen, J. Jepsen, T. Klassen, M. V. Lototskyy, K. Manickam, A. Montone, J. Puszkiel, S. Sartori, D. A. Sheppard, A. Stuart, G. Walker, C. J. Webb, H. Yang, V. Yartys, A. Züttel, M. Dornheim, *Int. J. Hydrogen Energy* **2019**, *44*, 7780–7808.
[4] R. W. P. Wagemans, J. H. van Lenthe, P. E. de Jongh, A. J. van Dillen, K. P. de Jong, *J. Am. Chem. Soc.* **2005**, *127*, 16675–16680.
[5] S. M. Lang, T. M. Bernhardt, D. M. Kiawi, J. M. Bakker, R. N. Barnett, U. Landman, *Angew. Chem. Int. Ed.* **2015**, *54*, 15113–15117; *Angew. Chem.* **2015**, *127*, 15328–15332.
[6] a) S. M. Lang, T. M. Bernhardt, D. M. Kiawi, J. M. Bakker, R. N. Barnett, U. Landman, *Phys. Chem. Chem. Phys.* **2016**, *18*, 15727–15737; b) J. P. Mojica-Sánchez, T. I. Zarate-López, J. M. Flores-Álvarez, J. Reyes-Gómez, K. Pineda-Urbina, Z. Gómez-Sandoval, *Phys. Chem. Chem. Phys.* **2019**, *21*, 23102–23110.
[7] S. Mauthe, I. Fleischer, T. M. Bernhardt, S. M. Lang, R. N. Barnett, U. Landman, *Angew. Chem. Int. Ed.* **2019**, *58*, 8504–8509; *Angew. Chem.* **2019**, *131*, 8592–8597.
[8] W. Ruan, A.-D. Xie, X.-G. Yu, D.-L. Wu, *Chin. Phys.* **2011**, *20*, 043104.
[9] A. Zanchet, A. Dorta-Urra, O. Roncero, F. Flores, C. Tablero, M. Paniagua, A. Aguado, *Phys. Chem. Chem. Phys.* **2009**, *11*, 10122–10131.
[10] S. J. Grabowski, F. Ruipérez, *Phys. Chem. Chem. Phys.* **2016**, *18*, 12810–12818.
[11] A. C. Tsipis, *Int. J. Hydrogen Energy* **2019**, *44*, 8341–8346.
[12] M. Habib, R. Sarkar, S. Biswas, A. Pramanik, P. Sarkar, S. Pal, *Phys. Chem. Chem. Phys.* **2019**, *21*, 7483–7490.
[13] a) G. Sánchez-Sanz, C. Trujillo, I. Alkorta, J. Elguero, *ChemPhysChem* **2019**, *20*, 1572–1580; b) G. Sánchez-Sanz, C. Trujillo, I. Alkorta, J. Elguero, *ChemPhysChem* **2020**, *21*, 2557–2563.
[14] a) P. R. Varadwaj, A. Varadwaj, H. M. Marques, K. Yamashita, *Sci. Rep.* **2019**, *9*, 50; b) S. J. Grabowski, *Crystals* **2021**, *11*, 5; c) E. Espinosa, E. Molins, *J. Chem. Phys.* **2000**, *113*, 5686–5694; d) E. Espinosa, E. Molins, C. Lecomte, *Chem. Phys. Lett.* **1998**, *285*, 170–173.
[15] a) I. Alkorta, M. Solimannejad, P. Provasi, J. Elguero, *J. Phys. Chem. A* **2007**, *111*, 7154–7161; b) I. Mata, I. Alkorta, E. Molins, E. Espinosa, *Chem. Eur. J.* **2010**, *16*, 2442–2452; c) G. Sánchez-Sanz, C. Trujillo, I. Alkorta, J. Elguero, *ChemPhysChem* **2012**, *13*, 496–503.
[16] a) J. Klein, H. Khartabil, J.-C. Boisson, J. Contreras-García, J.-P. Piquemal, E. Hénon, *J. Phys. Chem. A* **2020**, *124*, 1850–1860; b) C. Lefebvre, H. Khartabil, J.-C. Boisson, J. Contreras-García, J.-P. Piquemal, E. Hénon, *ChemPhysChem* **2018**, *19*, 724–735; c) C. Lefebvre, G. Rubez, H. Khartabil, J.-C. Boisson, J. Contreras-García, E. Hénon, *Phys. Chem. Chem. Phys.* **2017**, *19*, 17928–17936; d) M. Ponce-Vargas, C. Lefebvre, J.-C. Boisson, E. Hénon, *J. Chem. Inf. Model.* **2020**, *60*, 268–278; e) I. K. Petrushenko, H. F. Bettinger, *Phys. Chem. Chem. Phys.* **2021**, *23*, 5315–5324; f) I. K. Petrushenko, N. I. Tikhonov, K. B. Petrushenko, *Diamond Relat. Mater.* **2020**, *107*, 107905.
[17] C. Møller, M. S. Plesset, *Phys. Rev.* **1934**, *46*, 618–622.
[18] a) D. E. Woon, T. H. D. Jr, *J. Chem. Phys.* **1993**, *98*, 1358–1371; b) R. A. Kendall, T. H. D. Jr, R. J. Harrison, *J. Chem. Phys.* **1992**, *96*, 6796–6806.
[19] K. A. Peterson, C. Puzzarini, *Theor. Chem. Acc.* **2005**, *114*, 283–296.
[20] M. J. Frisch, G. W. Trucks, H. B. Schlegel, G. E. Scuseria, M. A. Robb, J. R. Cheeseman, G. Scalmani, V. Barone, G. A. Petersson, H. Nakatsuji, X. Li, M. Caricato, A. V. Marenich, J. Bloino, B. G. Janesko, R. Gomperts, B. Mennucci, H. P. Hratchian, J. V. Ortiz, A. F. Izmaylov, J. L. Sonnenberg, Williams, F. Ding, F. Lipparini, F. Egidi, J. Goings, B. Peng, A. Petrone, T. Henderson, D. Ranasinghe, V. G. Zakrzewski, J. Gao, N. Rega, G. Zheng, W. Liang, M. Hada, M. Ehara, K. Toyota, R. Fukuda, J. Hasegawa, M. Ishida, T. Nakajima, Y. Honda, O. Kitao, H. Nakai, T. Vreven, K. Throssell, J. A. Montgomery Jr., J. E. Peralta, F. Ogliaro, M. J. Bearpark, J. J. Heyd, E. N. Brothers, K. N. Kudin, V. N. Staroverov, T. A. Keith, R. Kobayashi, J. Normand, K. Raghavachari, A. P. Rendell, J. C. Burant, S. S. Iyengar, J. Tomasi, M. Cossi, J. M. Millam, M. Klene, C. Adamo, R. Cammi, J. W. Ochterski, R. L. Martin, K. Morokuma, O. Farkas, J. B. Foresman, D. J. Fox in *Gaussian 16 Rev. C.01*, Wallingford, CT, **2016**.
[21] T. Lu, F. Chen, *Comput. Chem.* **2012**, *33*, 580–592.
[22] a) R. F. W. Bader, M. T. Carroll, J. R. Cheeseman, C. Chang, *J. Am. Chem. Soc.* **1987**, *109*, 7968–7979; b) C. F. Matta, R. J. Boyd, *An Introduction to the Quantum Theory of Atoms in Molecules*, Wiley-VCH Verlag, Germany, **2007**, 1–34.
[23] a) M. Núñez, D. G. Vlachos, *J. Chem. Phys.* **2015**, *142*, 044108; b) A. Hashemi, M. Núñez, P. Plecháč, D. G. Vlachos, *J. Chem. Phys.* **2016**, *144*, 074104.

Manuscript received: May 13, 2021
Revised manuscript received: June 30, 2021